JOURNAL OF AIRCRAFT
Vol. 32, No. 1, January–February 1995

Study of the Droplet Spray Characteristics of a Subsonic Wind Tunnel

Michael B. Bragg* and Abdollah Khodadoust†
University of Illinois at Urbana–Champaign, Urbana, Illinois 61801

A finite difference, two-dimensional potential flow solver, and a three-dimensional particle trajectory code have been written to compute water droplet trajectories in a subsonic incompressible flow wind tunnel. This method was used to study the spray cloud in the test section of a two-dimensional wind tunnel resulting from the injection of a distribution of water droplets in the settling chamber ahead of the inlet. The results of this computational study showed that the trajectories of the larger water droplets were affected by the droplet inertia and gravity more dramatically than that for the smaller particles. The calculated liquid water content across the test section indicated a high concentration near the tunnel centerline. The largest droplets were present at the test section only in the center one-third of the wind tunnel, whereas the smaller droplets spanned almost the entire test section width. This resulted in a computed droplet size distribution skewed toward the larger droplets in comparison with the initial Langmuir-D distribution. The distribution of particle sizes and concentrations required at the droplet injection point in the settling chamber for a Langmuir-D distribution of uniform liquid water content in the center third of the test section was computed.

Nomenclature

A = droplet trajectory stream tube area
C_D = droplet drag coefficient
CR = tunnel contraction ratio, H_i/H_{TS}
Fr = Froude number, $U_{TS}/\sqrt{H_i g}$
g = gravitational acceleration constant
H = tunnel width
H_S = flowfield total head, P_{total}/ρ
K = droplet inertia parameter, $\sigma\delta^2 U_{TS}/18H_i\mu$
R_U = droplet freestream Reynolds number, $\rho U_{TS}\delta/\mu$
S = stream function
t = time
U = average flow speed at an x location
u = local flow speed in x direction
v = local flow speed in y direction
x, y, z = tunnel Cartesian coordinate system
δ = droplet diameter
η = droplet nondimensional position
ρ = air density
σ = droplet density
τ = nondimensional time, Ut/H_i
ω = flow vorticity

Subscripts
i = tunnel inlet value
TS = tunnel test section value

Superscripts
$\bar{}$ = vector quantity
$\dot{}$ = first derivative with respect to τ
$\ddot{}$ = second derivative with respect to τ

Received Feb. 23, 1994; revision received May 28, 1994; accepted for publication May 30, 1994.

*Associate Professor, Department of Aeronautical and Astronautical Engineering. Associate Fellow AIAA.
†Postdoctoral Research Associate, Department of Aeronautical and Astronautical Engineering. Student Member AIAA.

Introduction

DURING flight in adverse weather conditions, an aircraft is subjected to water droplet impingement. Given the proper conditions, the impinging water may freeze on the flight surfaces, reducing their aerodynamic efficiency. To provide the aircraft all-weather capability, anti-icing and de-icing systems are used on the leading edge of the most flight-critical surfaces. In order to determine the extent of the surface that is to be protected by the anti- or de-icing equipment, and the amount of protection needed, it is necessary to know the details of the water droplet impingement on the surface.

Computational methods have been developed to calculate water droplet impingement on airfoils and wings.[1–6] Wind-tunnel tests have been conducted in icing tunnels to measure impingement characteristics for code validation.[7–9] While the existing codes calculate the impingement efficiency in free air, the validation studies are performed in wind tunnels where the tunnel walls can affect the droplet trajectories. The wall effects have been found to be small and within the limits of experimental error for most two-dimensional airfoil testing in a typical subsonic wind-tunnel test section, without accounting for the upstream inlet contraction effects on the water droplet trajectories.[10] Effects of the wind-tunnel walls on the computed trajectories in a three-dimensional flowfield with a reflection-plane mounted rectangular wing are currently under investigation.[11] These early three-dimensional results show trends similar to the two-dimensional wall effects.

The previous wall-effects studies[10,11] assumed that the wind-tunnel spray system had been adjusted to provide a uniform cloud in the test section with regards to both droplet size and liquid water content. These studies then examined the effect of the wind-tunnel walls on the aerodynamics of the airfoil or wing and how this affected its droplet impingement characteristics. This study is intended to provide insight into how the wind-tunnel contraction affects the water droplet cloud in the test section, and how the initial spray cloud can be modified to provide a uniform test section cloud.

Numerical Formulation

Flowfield

The flowfield solution technique employed here was used by Coirier[12,13] to study the effect of screens on two-dimensional inlets using a finite difference method for subsonic

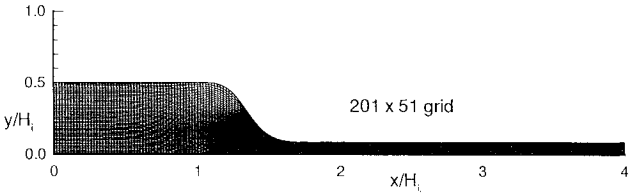

Fig. 1 Computational grid in the physical domain.

inviscid incompressible flow. The stream function S satisfying the continuity equation is defined such that the velocity field is given by

$$u = \frac{\partial S}{\partial y} \qquad v = -\frac{\partial S}{\partial x} \tag{1}$$

Substitution into the momentum equation leads to the following Poisson equation:

$$S_{xx} + S_{yy} = \frac{\partial H_S}{\partial S} \tag{2}$$

where $\partial H_S/\partial S$ is defined as the source term $P(S)$. Introducing a Laplace equation of a different variable N as

$$N_{xx} + N_{yy} = 0 \tag{3}$$

and inverting the Poisson system of Eqs. (2) and (3) yields the following elliptic partial differential equations that are solved in the rectangular computational domain:

$$AX_{ss} - 2BX_{sn} + CX_{nn} = -J^2(PX_s) \tag{4}$$

$$AY_{ss} - 2BY_{sn} + CY_{nn} = -J^2(PY_s) \tag{5}$$

$$A = X_n^2 + Y_n^2 \tag{6}$$

$$B = X_s X_n + Y_s Y_n \tag{7}$$

$$C = X_s^2 + Y_s^2 \tag{8}$$

$$J = X_s Y_n - X_n Y_s \tag{9}$$

These equations determine the X and Y locations of the constant S (streamlines) and constant N lines in the physical domain. The transformation yields the flow streamlines, thus, the generation of the elliptic grid yields the velocity field using Eq. (1). Figure 1 shows the computational grid in the physical domain with the inflow and outflow planes set one inlet length upstream and downstream of the inlet and exit planes, respectively. This boundary placement will allow the flow angle distribution to smoothly approach zero at the inflow and outflow planes.

Equations (4) and (5) were solved using second-order central and one-sided finite differences in a successive line-relaxation method. The value of the S on the upper and lower boundaries and the flow angle at the inflow and outflow planes served as the boundary conditions on the rectangular computational domain. The value of the total head gradient or $P(S)$ was set to zero for this study, except for the special case described in the Code Verification section.

Particle Trajectory

Assuming a low concentration of spherical droplets of constant mass, Newton's second law of motion in nondimensional form yields[2,14]

$$\ddot{\eta} = \frac{1}{K}\left(\frac{C_D R}{24}\right)\left(\frac{\bar{u}}{U_{TS}} - \dot{\eta}\right) + \frac{1}{Fr^2}\frac{\bar{g}}{g} \tag{10}$$

where the droplet Reynolds number is

$$R = R_U\left|(\bar{u}/U_{TS}) - \dot{\eta}\right| \tag{11}$$

The velocity $\bar{u}/U$ in Eqs. (10) and (11) are determined by interpolation of velocities obtained from the finite difference solution of the flowfield. The particle drag is calculated by the method of Langmuir and Blodgett,[15] which yields the following form in the trajectory equation above:

$$\frac{C_D R}{24} = 1.0 + 0.197R^{0.63} + 2.6 \times 10^{-4}R^{1.38} \tag{12}$$

Given the droplet initial conditions in addition to the free-stream and droplet size data, the trajectory equation is numerically solved by a predictor-corrector scheme due to Gear.[16]

In two dimensions, the droplet stream tube areas A_i and A_{TS} at the inlet and test section, respectively, are obtained from adjacent droplet trajectories. Then, through the principle of mass conservation

$$\mathrm{LWC}_{TS} = \mathrm{LWC}_i \frac{U_i}{U_{TS}} \frac{A_i}{A_{TS}} \tag{13}$$

relates the liquid water content (LWC) in the wind-tunnel inlet LWC_i, and test section LWC_{TS}, where droplet evaporation is ignored. The droplet velocity at the inlet plane and the test section plane are assumed equal to the corresponding x components of the tunnel velocity. Assuming uniform flow at the inlet and test section planes, the velocity ratio is U_i/U_{TS}, and is equal to the wind-tunnel contraction ratio CR.

Code Verification

The verification of the code was carried out in two steps. First, the flowfield calculations were verified, and in the second step, trajectory computations were verified. An initial check was performed using a 161 by 31 grid to ensure that mass was conserved within the tunnel. In an incompressible flow, the increased velocity in the test section is proportional to the contraction ratio of the tunnel inlet. The average u component of velocity, nondimensional with respect to the test section velocity, should be $1/CR$ at the wind-tunnel inlet. The average velocities at the inflow plane were within 0.047%, proving that mass within the wind tunnel was indeed being conserved.

A second test of the flowfield was also performed. For an arbitrary two-dimensional contraction with constant vorticity everywhere in the flowfield, the analytical solution for the u-velocity profile may be obtained at the inflow plane by[12]

$$u_1 = -\omega y_1 + (\omega H_i/2) + (1/CR) \tag{14}$$

and at the outflow plane by

$$u_2 = -\omega y_2 + (\omega H_i/2CR) + 1 \tag{15}$$

The subscripts 1 and 2 denote conditions at the inflow and the outflow planes, respectively, and H_i denotes the inlet width. The v velocity is set to zero by imposing the Neumann boundary condition at the inflow and outflow planes, and P on the right side of Eq. (2) is set to $-\omega$. Figures 2 and 3 show the comparison of the inflow and outflow u-velocity profiles for two values of vorticity, $\omega = -0.1$ and -0.3. Examination of the profiles shows that the computed and predicted profiles compare quite well. The computed and the predicted profiles agreed to within 0.0049%.

The trajectory computations were verified by comparing the trajectories computed by the present method to those computed by the method of Wells and Bragg[10] in a rectangular duct with no contraction effects. The method of Ref. 10 uses

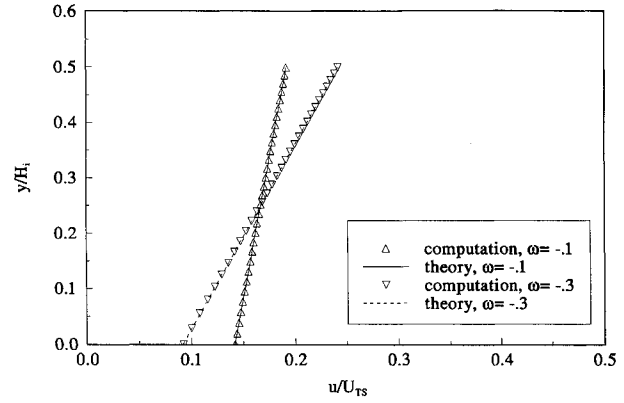

Fig. 2 Comparison of inflow velocity profiles for $\omega = -0.1$ and -0.3.

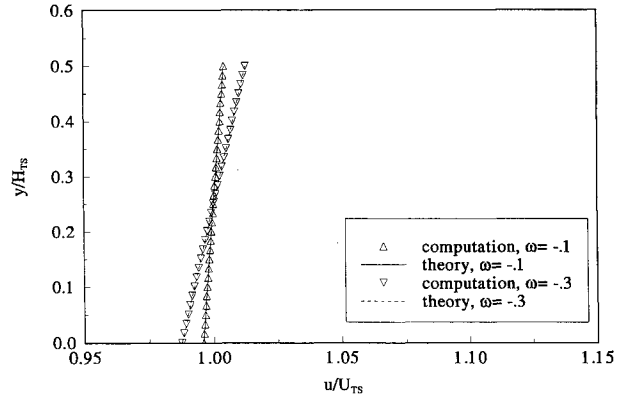

Fig. 3 Comparison of outflow velocity profiles for $\omega = -0.1$ and -0.3.

a panel method to obtain the flowfield coupled with a similar droplet trajectory calculation method. For example, a 20.36-μm-diam water droplet was released at the beginning of the duct with the same streamwise velocity as the flow (100 mph), and a crossflow velocity of 40 mph. Both methods of computation show the 20.36-μm droplet loses the crossflow velocity component rapidly and maintains only a streamwise flow component 0.0231 s after injection in the tunnel. The computed y location of the droplet at a given x location compared to within 0.0004% during the first 0.0231 s after injection.

Results and Discussion

The droplet trajectory method described above has been used to study the droplet trajectory characteristics and the resulting spray cloud in the test section of a two-dimensional subsonic wind tunnel. The tunnel contraction takes place in the xy plane, with gravity acting in the $(-z)$ direction, which is into the page in Fig. 1. The tunnel has a contraction ratio of 6, and a test section width and length of 10 and 60 in., respectively. The test section velocity U_{TS} was set equal to 175 mph. The characteristics of the spray nozzles that are mounted in the tunnel were used to determine a suitable range of droplet sizes for this analysis. Operating at a pressure ratio of 0.65, the nozzles produce water droplets with a median volumetric diameter (MVD) of 20.36 μm.[8] Assuming a Langmuir-D distribution (Table 1), seven droplet sizes ranging from 6.31 to 45.19 μm were considered.

All calculations were performed using a 201 by 51 grid. Droplet trajectories were initiated at the same x location, $x/H_i = 0.8$, varying in y location across the tunnel width from the centerline to $y/H_i = 0.49$, or until the droplet hit the inlet wall after release. Since the tunnel is symmetric, no trajectories were calculated for negative y values. The initial droplet velocity was set equal to the tunnel velocity at the injection point. Droplet trajectories were terminated when the test section location $x/H_i = 2.5$ was reached.

Table 1 Langmuir-D droplet distribution for MVD = 20.36 μm

δ/MVD	δ, μm	Mass %
0.31	6.31	5
0.52	10.58	10
0.71	14.46	20
1.00	20.36	30
1.37	27.89	20
1.74	35.42	10
2.22	45.19	5

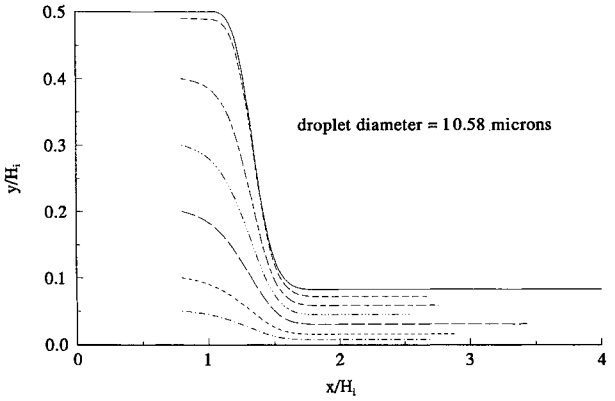

Fig. 4 Droplet trajectories for the 10.58-μm droplet.

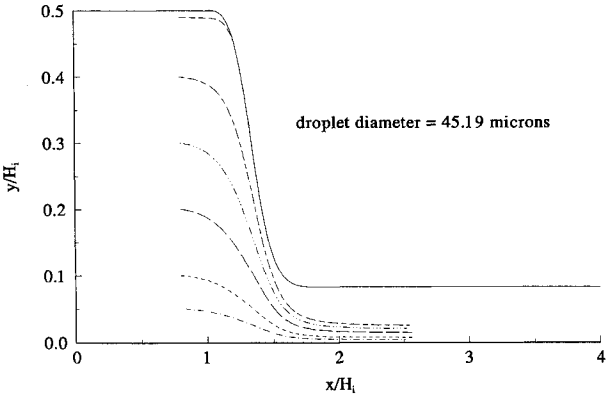

Fig. 5 Droplet trajectories for the 45.19-μm droplet.

Figure 4 shows the computed trajectories for the 10.58-μm droplets. These droplets follow the flowfield streamlines more closely than the larger droplets whose trajectories are shown in Fig. 5. Due to the larger droplet size and mass, the droplets do not negotiate the turn in the tunnel contraction just prior to the test section. The droplets' inertia carry them near the tunnel centerline downstream of the contraction. The larger droplets have more inertia, and as a result, their ability to follow the flowfield in regions of high-velocity gradients were reduced in comparison with smaller droplets.

Since the droplets have size and mass, it is anticipated that their motion will be affected by gravity. Droplet fallout, defined as the z distance traveled by the droplet, is shown in Fig. 6. The 10.58- and 45.19-μm droplets were released at the same x and z, but at different y locations. The droplets released at $y/H_i = 0.40$ take more time to reach the test section than the droplets released at $y/H_i = 0.05$. Consequently, the fallout for the droplet trajectories originating at $y/H_i = 0.40$ was larger. The maximum fallout is computed to be 0.165 in. for the 45.19-μm droplet over the 8 ft distance

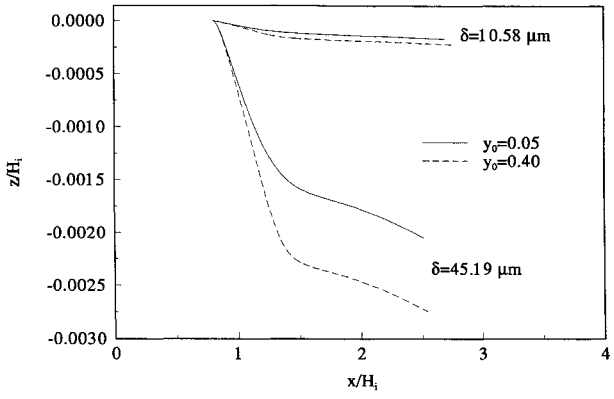

Fig. 6 Comparison of the computed fallout for the 10.58- and 45.19-μm droplets.

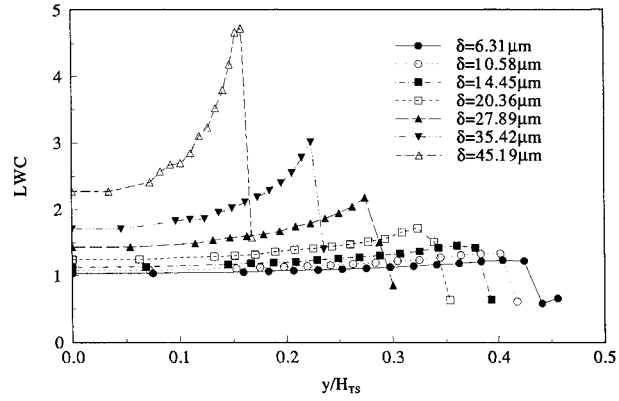

Fig. 7 LWCs across the tunnel test section for monodisperse sprays with the inlet LWC = 1.

from the nozzle location in the inlet to the test section. The maximum fallout for the smaller droplet is computed to be 0.0133 in. Neither of these fallout distances is considered significant, particularly since fallout for this two-dimensional tunnel is in the direction perpendicular to the plane of the contraction.

In order to investigate the mass distribution across the test section, the LWC in the test section must be estimated. The trajectories for seven droplet sizes based on the Langmuir-D distribution were computed. The LWC in the test section for the seven droplet sizes are shown in Fig. 7. The distributions shown are not weighted by the Langmuir-D distribution. They show the LWC for each droplet size as if a separate monodisperse cloud was tested at each droplet size. The results reflect the trend seen in the individual particle trajectories shown in Figs. 4 and 5. The smaller droplets are able to follow the flowfield closely and, therefore, their LWC across the test section is nearly uniform. The smallest droplet at a diameter of 6.31 μm has a LWC near 1 at the centerline increasing slightly as the tunnel wall is approached. The LWC goes to zero beyond approximately $y/H_{TS} = 0.43$, where even this small droplet cannot follow the flow due to the high gradients in the vicinity of the rapid contraction coming into the test section. As the droplet size is increased (Fig. 7), the LWC at the centerline increases and the reduction in LWC to zero occurs closer to the tunnel centerline. This is of course due to the increasing inertia of the droplets. For the largest droplet tested at 45.19 μm, the LWC predicted was 2.27 at the centerline with a rapid increase to 4.73 before dropping to zero at $y/H_{TS} = 0.172$.

Test Section Cloud Resulting from a Uniform Inlet Cloud

Now consider a uniform initial cloud at the nozzle plane that has a Langmuir-D distribution and LWC = 1. Table 1 gives the droplet sizes for a Langmuir-D distribution for a MVD = 20.36 μm and the corresponding percentage of the total mass represented by each droplet. If the tunnel walls had no effect on the droplet trajectories, a Langmuir-D distribution with LWC = 1 would be expected across the entire test section. However, due to the tunnel wall effects in the inlet, the LWC and droplet size distribution will vary across the test section. The effect of the tunnel walls on the total LWC across the test section is plotted in Fig. 8. The curve is not as smooth as might be expected since only seven droplets were chosen to represent the distribution, as is typically done in icing calculations. The LWC is greater than one in the center of the tunnel due to the increased concentration of large droplets, and is fairly constant at a LWC $\approx$ 1.35 until $y/H_{TS} \approx 0.20$. From this location out towards the tunnel wall the LWC drops rapidly due to the absence of the larger droplets. An LWC = 1.0 is reached at approximately $y/H_{TS} = 0.30$, and no mass is predicted in the tunnel beyond $y/H_{TS} = 0.430$.

In an experimental study measuring ice accretion or droplet impingement, the test section LWC is measured using a reference collector or other device. During the facility calibration, the placement of the nozzles in the inlet is adjusted to provide uniform LWC or ice accretion over as large a portion of the test section as possible. Thus, a usable cloud of uniform LWC in the center of the tunnel is available for testing, with the effect of the tunnel walls on LWC essentially removed. However, the effect of the tunnel walls on the droplet size distribution is not so easily measured or corrected.

Figure 9 shows the mass, made nondimensional with respect to the total mass, for each of the seven droplet sizes at nine locations across the tunnel test section. Also shown is the initial Langmuir-D droplet distribution at the inlet from Table 1. The droplet size distributions at the tunnel centerline and

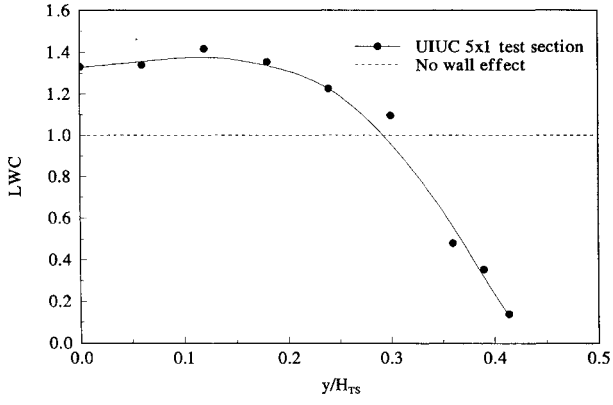

Fig. 8 LWC across the test section with the inlet LWC = 1 and a Langmuir-D distribution.

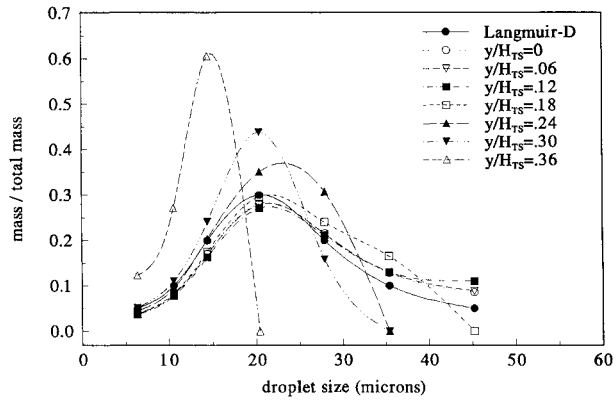

Fig. 9 Droplet size distributions at several locations across the test section with the inlet LWC = 1 and a Langmuir-D distribution.

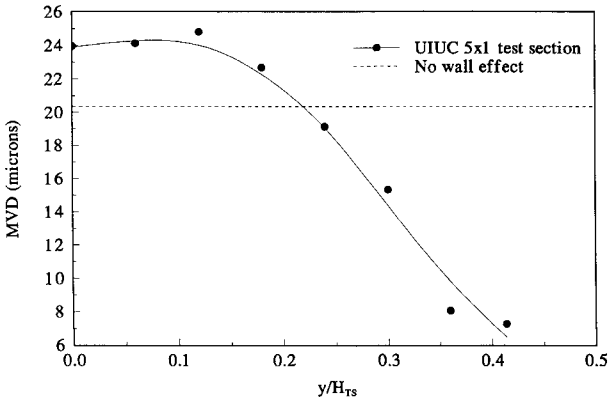

Fig. 10 Effective MVD across the test section with the inlet LWC = 1 and a Langmuir-D distribution.

the next three stations are very similar. Although shifted to the right due to the presence of more large droplets than that found in the Langmuir-D distribution, only a small variation with tunnel location is seen in this center area of the tunnel. This region corresponds roughly to the region of constant LWC in Fig. 8. As would be expected from the results of Fig. 7, the amount of mass in the distributions from the smaller droplets increases significantly as the tunnel wall is approached.

Since the droplet size distribution varies from that which yields a MVD of 20.36 μm based on the Langmuir-D distribution, it would be logical to calculate new MVDs based on the new distributions. In order to determine the new MVDs for each y station across the test section, the fraction of total LWC for each y station is added up in cumulative fashion as a function of droplet size. The MVD droplet divides the size distribution such that 50% of the volume is made up of droplets smaller than the MVD droplet and the remaining 50% are droplets larger than the MVD droplet. The MVDs across the test section are shown in Fig. 10. For locations near the tunnel centerline ($y/H_{TS} < 0.220$), the MVD is larger than 20.36 μm. Outside of this range, only the smaller droplets are present and, therefore, the effective MVD is lower than 20.36 μm. This expected redistribution or sorting of the droplets is due to the effects of the tunnel contraction. As noted from the droplet size distributions in Fig. 9, the MVD near the tunnel centerline is fairly constant at a value of about 24 μm.

Inlet Spray to Provide a Uniform Test Section Cloud

Using the same trajectory information that was presented in Figs. 7–10, the spray cloud characteristics required at the inlet to produce the desired cloud in the test section can be determined. First, as in Fig. 7, consider seven separate monodisperse clouds. Figure 11 shows the initial LWC across the inlet that would be required to produce a LWC = 1 in the test section for each separate droplet size. From Eq. (13) it is easily seen that these values are just the reciprocal of those in Fig. 7. Therefore, as the droplet size is increased and the mass is more concentrated in the center of the tunnel due to the wall effect, the LWC at the inlet to provide LWC = 1 in the test section is reduced. The difference between the 6.31- and the 45.19-μm droplet is large, with the smaller droplet having a LWC = 0.967 at the inlet centerline, while the largest droplet has only an LWC value of 0.440.

It would be useful in designing the inlet spray system to know what inlet cloud conditions are required to produce the desired test section cloud. A test section cloud with a Langmuir-D distribution and LWC = 1 across the test section would be highly desirable. Unfortunately, due to the inlet wall effects, such a cloud across the test section is not possible. From Fig. 7 it is seen that the larger droplets only exist in the center part of the test section. Therefore, assume instead, that a test section cloud is desired, where at each location each droplet size exists in an absolute concentration as given by the Langmuir-D distribution. In such a cloud the LWC will be 1, and a Langmuir-D distribution will exist, only over the center section of the test section where all droplet sizes are present. As the cloud is examined further out towards the wall, the LWC will be reduced as the larger droplets are no longer present and the smaller droplets continue to be present in the same absolute concentration. Therefore, for this tunnel a Langmuir-D cloud with LWC = 1 will only be produced in the test section for $y/H_{TS} < 0.172$.

Figures 12 and 13 show the inlet spray cloud characteristics for the test section conditions described above. In Fig. 12, the total LWC is seen to decrease as the wall is approached

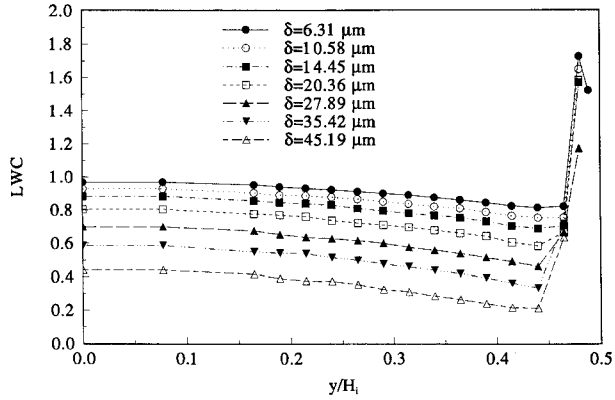

Fig. 11 LWC across the inlet to provide LWC = 1 in the test section for various droplet sizes.

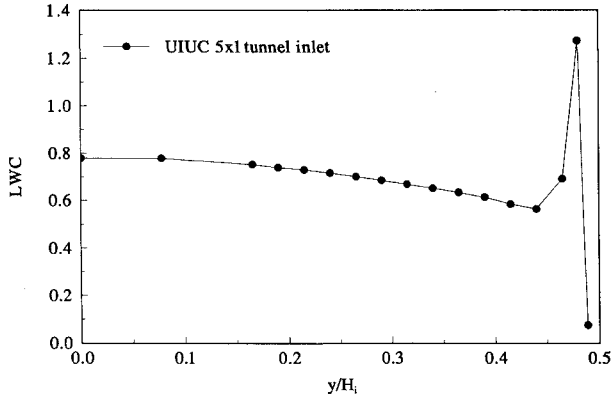

Fig. 12 Variation of LWC across the inlet to provide LWC = 1 and a Langmuir-D distribution across the test section from y/H_{TS} = 0 to ±0.17.

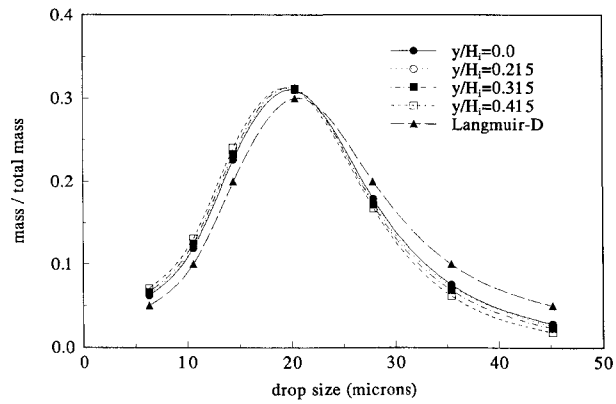

Fig. 13 Droplet size distributions required at several inlet stations to provide LWC = 1 and a Langmuir-D distribution across the test section from y/H_{TS} = 0 to ±0.17.

following the trends of Fig. 11. This is nearly linear until the trajectories very near the wall distort the outer part of the curve. Figure 13 shows the mass of water required in the inlet cloud, made nondimensional with respect to the total LWC, by droplet size at four locations across the inlet. The Langmuir-D distribution is also shown in Fig. 13 for comparison. While there is some variation across the inlet, the droplet size distributions are very close. Each has more small droplets and fewer larger droplets than the Langmuir-D distribution. For example, at $y/H_i = 0.215$, the required inlet distribution has about one-half the mass of 45.19-μm droplets as a Langmuir-D distribution, and 27% more mass in 6.31-μm droplets. The MVDs of the inlet cloud decrease slightly while moving from the centerline towards the wall, reflecting a small increase in small droplets and decrease in large droplets. The MVDs are 18.98, 18.82, 18.62, and 18.28 μm from $y/H_i = 0$ to 0.415, respectively.

Conclusions

A computational method was presented to calculate water droplet trajectories and the droplet spray cloud characteristics in a two-dimensional incompressible wind tunnel. The flowfield in the tunnel is generated through a finite difference solution of the governing Poisson equation that also generates the computational grid. Trajectories are calculated using a Lagrangian method where the flowfield velocities are interpolated from the grid. The method is demonstrated by calculating droplet trajectories and spray cloud characteristics inside a two-dimensional subsonic wind tunnel.

Results were presented for a Langmuir-D distribution with a 20.36-μm MVD droplet, resulting in seven droplet sizes ranging from 6.31 to 45.19 μm in diam. The computed droplet fallout due to gravity was negligible for all droplet sizes. The computed trajectories for the droplets showed that the lighter particles followed the flow more closely than the heavier droplets in regions of high flow gradient, as expected. The contraction region of the tunnel presents such a region. The larger droplets were not able to negotiate the large velocity gradients immediately upstream of the test section, and as a result, an increased concentration of large droplets near the tunnel centerline was observed. No large droplets were predicted in approximately the outside two-thirds of the tunnel test section.

The test section cloud characteristics were predicted assuming an initial cloud of LWC = 1 with a Langmuir-D distribution of water droplets with a MVD = 20.36 μm. Near the test section centerline the LWC was increased to approximately 1.35 and the MVD was approximately 24 μm. These values were relatively constant over the center third of the tunnel test section, then both the LWC and MVD decrease further out towards the tunnel wall due to the absence of the larger droplets. Therefore, a relatively small region of a uniform spray cloud suitable for testing exists centered on the tunnel centerline with elevated values of LWC and MVD relative to the inlet conditions.

The cloud characteristics required in the inlet to produce a uniform cloud of LWC = 1 and MVD = 20.36 μm were calculated. However, since the flowfield gradients in the inlet prevent any large droplets from reaching the outer region of the test section, only the center of the test section where large droplets are present could be controlled. Returning the cloud in the center of the test section to the desired MVD and LWC can be easily accomplished numerically by reducing the MVD and LWC in the inlet spray. In this case an MVD on the inlet centerline of 18.9 μm and an LWC of 0.8 was required. These values decrease slightly off the centerline until the wall region is reached.

This analysis represents an exploratory study of the tunnel contraction effects on the droplet motion and distribution in a subsonic incompressible wind tunnel. Tunnel wall effects were found to have a significant effect on droplet distribution in the test section. The primary effect was caused by the large flowfield gradients due to the rapid contraction in the inlet just ahead of the test section. Due to their inertia the larger droplets could not negotiate this turn and are, therefore, concentrated near the test section centerline. This means that the region of uniform cloud characteristics across the test section is limited due to the behavior of the large droplets. In an actual icing tunnel, the region of uniform spray may be significantly larger than that predicted in this study. This could be due to a different inlet geometry, or nozzle/spray bar characteristics and turbulent diffusion that were not modeled in this study.

The calculation method presented here could be useful in optimizing a wind-tunnel inlet design to achieve a larger uniform cloud in the test section while still maintaining acceptable aerodynamic performance. This method could also be used to help position spray nozzles for a uniform test section cloud. The current method can easily handle detailed spray nozzle characteristics and a nonuniform initial cloud distribution if such information is available. Extending the method to model three-dimensional inlets, the turbulent wake behind the spray bars and droplet evaporation effects would improve the usefulness of the model.

Acknowledgment

This work was supported in part by B.F.Goodrich De-Icing Systems, Uniontown, Ohio.

References

[1]Norment, H. J., "Calculation of Water Drop Trajectories to and About Arbitrary Three-Dimensional Bodies in Potential Airflow," NASA CR 3291, Aug. 1980.

[2]Bragg, M. B., "Rime Ice Accretion and Its Effect on Airfoil Performance," Ph.D. Dissertation, Ohio State Univ., Columbus, OH, Aug. 1981; also NASA CR 165599, March 1982.

[3]Gent, R. W., "Calculation of Water Droplet Trajectories About an Airfoil in Steady, Two-Dimensional, Compressible Flow," Royal Aircraft Establishment TR 84060, June 1984.

[4]Lozowski, E. P., and Oleskiw, M. M., "Computer Modeling of Time-Dependent Rime Icing in the Atmosphere," U.S. Army Corps of Engineers Cold Regions Research and Engineering Lab. Rept., CRREL 83-2, Jan. 1983.

[5]Kim, J. J., "Computational Particle Trajectory Analysis on a Three-Dimensional Engine Inlet," AIAA Paper 85-0411, Jan. 1985.

[6]Ruff, G. A., and Berkowitz, B., "User's Manual for the NASA Lewis Ice Accretion Code (LEWICE)," NASA CR-185129, 1990.

[7]Gelder, T. F., Smyers, W. H., and Von Glahn, U., "Experimental Droplet Impingement on Several Two-Dimensional Airfoils with Thickness Ratios of 6 to 16 Percent," NACA TN 3839, 1956.

[8]Papadakis, M., Elangonan, R., Freund, G. A., Jr., Breer, M., Zumwalt, G. W., and Whitmer, L., "An Experimental Method for Measuring Water Droplet Impingement Efficiency on Two- and Three-Dimensional Bodies," NASA CR 4257, Nov. 1989.

[9]Tenison, G., Bragg, M. B., and Farag, K., "A Comparison of a Droplet Impingement Code to Icing Tunnel Results," AIAA Paper 90-0670, Jan. 1990.

[10]Wells, S. L., and Bragg, M. B., "A Computational Method for Calculating Droplet Trajectories Including the Effects of Wind Tunnel Walls," AIAA Paper 92-0642, Jan. 1992.

[11]Farag, K., and Bragg, M. B., "The Effects of Wind Tunnel Walls on Droplet Trajectories in the Vicinity of a 3D Wing," AIAA Paper 94-0644, Jan. 1994.

[12]Coirier, W. J., "A Computational Method for the Analysis of Low Speed Wind Tunnel Inlets with Screens, Using an Application of Elliptic Grid Generation," M.S. Thesis, Ohio State Univ., Columbus, OH, March 1985.

[13]Coirier, W. J., and Bragg, M. B., "Computational Method for Screened Two-Dimensional Wind Tunnel Inlets," *Journal of Aircraft*, Vol. 24, No. 4, 1987, pp. 281–283.

[14]Bragg, M. B., "A Similarity Analysis of the Droplet Trajectory Equation," *AIAA Journal*, Vol. 20, No. 12, 1982, pp. 1681–1686.

[15]Langmuir, I., and Blodgett K., "A Mathematical Investigation of Water Droplet Trajectories," Army Air Force Technical Rept., AAFTR 5418, Feb. 1946.

[16]Gear, C. W., "DIFSUB for Solution of Ordinary Differential Equations," *Association for Computing Machinery*, Vol. 14, March 1971, pp. 785–790.